Tomographic fluorescence reconstruction by a spectral projected gradient pursuit method

Jinzuo Ye[a], Yu An[b],Yamin Mao[a],Shixin Jiang[b], Xin Yang[a], Chongwei Chi[*a], Jie Tian[*a]
[a] Key Laboratory of Molecular Imaging of Chinese Academy of Sciences, Institute of Automation, Chinese Academy of Sciences, Beijing 100190, China; [b] Beijing Jiaotong University, School of Computer and Information Technology, Department of Biomedical Engineering, Beijing 100044, China

ABSTRACT

In vivo fluorescence molecular imaging (FMI) has played an increasingly important role in biomedical research of pre-clinical area. Fluorescence molecular tomography (FMT) further upgrades the two-dimensional FMI optical information to three-dimensional fluorescent source distribution, which can greatly facilitate applications in related studies. However, FMT presents a challenging inverse problem which is quite ill-posed and ill-conditioned. Continuous efforts to develop more practical and efficient methods for FMT reconstruction are still needed. In this paper, a method based on spectral projected gradient pursuit (SPGP) has been proposed for FMT reconstruction. The proposed method was based on the directional pursuit framework. A mathematical strategy named the nonmonotone line search was associated with the SPGP method, which guaranteed the global convergence. In addition, the Barzilai-Borwein step length was utilized to build the new step length of the SPGP method, which was able to speed up the convergence of this gradient method. To evaluate the performance of the proposed method, several heterogeneous simulation experiments including multisource cases as well as comparative analyses have been conducted. The results demonstrated that, the proposed method was able to achieve satisfactory source localizations with a bias less than 1 mm; the computational efficiency of the method was one order of magnitude faster than the contrast method; and the fluorescence reconstructed by the proposed method had a higher contrast to the background than the contrast method. All the results demonstrated the potential for practical FMT applications with the proposed method.

Keywords: fluorescence molecular tomography, image reconstruction techniques, inverse problems, spectral projected gradient pursuit

1. INTRODUCTION

Fluorescence molecular imaging (FMI) has played an increasingly important role in biomedical research of pre-clinical and clinical areas [1-3]. Fluorescence molecular tomography (FMT), which is derived from FMI, is an important imaging modality which is able to quantify several important fluorescent proteins and localize the fluorescent sources inside small animals. It has the potential to elucidate molecular and cellular signatures or pathways *in vivo* by using specific small animal models, thus promotes related researches about cancer and accelerates drug development [4-6].

However, FMT is usually an ill-posed inverse problem, because the measurements of photon distribution on the surface of small animals are limited. Besides, FMT is also an ill-conditioned inverse problem since it is unstable and sensitive to noise caused by CCD measurement errors and data discretization errors [7]. To overcome these difficulties and to obtain a reasonable solution, appropriate constraints on the solution should be incorporate into the FMT reconstruction. The regularization strategies are introduced by several researchers to make the solutions of FMT and other optical tomographic problems stable and less sensitive to perturbations. Tikhonov regularization is one of the most popular and commonly used strategies [8, 9]. However, it usually results in an over-smoothed solution of the FMT problem and it does not take advantage of the sparsity of the source distribution. For FMT, the domains of the fluorescent sources are usually small and sparse compared with the entire reconstruction domain, especially in mouse models with early-stage tumors. This can be considered as *a priori* information for FMT and thus sparse regularization can be incorporated into FMT to promote the sparsity of the solution [10, 11]. A straightforward way to incorporate sparsity regularization is to

[*] Chongwei Chi, Email: chongwei.chi@ia.ac.cn; Jie Tian, Email: tian@ieee.org

Multimodal Biomedical Imaging X, edited by Fred S. Azar, Xavier Intes, Proc. of SPIE Vol. 9316, 931604

doi: 10.1117/12.2077165

use the l_0-norm regularization. However, the FMT problem incorporated with l_0-norm regularization becomes NP-hard and is difficult to be solved efficiently. Inspired by the theory of compressive sensing (CS), several researchers proposed various algorithms incorporated with l_1-norm regularization to solve the FMT problem in recent years[7, 12-14], such as the sparsity adaptive subspace pursuit method and the iterated shrinkage based method with l_1-norm (IS_L1) [13, 14].

Continuous efforts to develop more practical and efficient methods for FMT reconstruction are still needed [15]. In this paper, a method based on spectral projected gradient pursuit (SPGP) has been proposed for FMT reconstruction. The proposed method was based on the directional pursuit framework. A mathematical strategy named the nonmonotone line search was associated with the SPGP method, which guaranteed the global convergence. In addition, the Barzilai-Borwein step length was utilized to build the new step length of the SPGP method, which was able to speed up the convergence of this gradient method. To evaluate the performance of the proposed method, several heterogeneous simulation experiments including multisource cases as well as comparative analyses have been conducted. The results demonstrated that: the proposed method was able to achieve satisfactory source localizations with a bias less than 1 mm; the computational efficiency of the method was one order of magnitude faster than the conjugate gradient based method with l_2 norm (CG_L2); and the fluorescence reconstructed by the proposed method had a higher contrast to the background than the contrast method. All the results demonstrated the potential for practical FMT application with the proposed method.

2. METHODS

2.1 Photon propagation model

Photon propagation in biological tissues can be described using the radiative transfer equation (RTE). For photon propagation in biological tissues with the near-infrared spectral window, scattering is the main phenomenon over absorption. Thus the diffusion equation (DE), which is a low-order approximation of the RET, is usually used to explain photon propagation in highly scattering media [16]. For FMT with continuous wave (CW) excitation point sources, the following coupled DEs have been widely used to depict photon propagation:

$$\begin{cases} \nabla\cdot\left[D_x(r)\nabla\Phi_x(r)\right]-\mu_{ax}(r)\Phi_x(r)=-\Theta\delta(r-r_l) \\ \nabla\cdot\left[D_m(r)\nabla\Phi_m(r)\right]-\mu_{am}(r)\Phi_m(r)=-\Phi_x(r)\eta\mu_{af}(r) \end{cases} \quad (r\in\Omega) \tag{1}$$

where Ω denotes the domain of the problem; r denotes a certain position in the domain Ω; subscripts x and m denote the excitation and emission wavelengths, respectively; $\Phi_{x,m}$ denotes the photon flux density; $D_{x,m}$ denotes the diffusion coefficient and $\mu_{ax,am}$ denotes the absorption coefficient. In the forward model, the excitation light spot is usually modeled as an isotropic point source $\Theta\delta(r - r_l)$, which is located one mean free path of photon transport beneath the surface. Θ denotes the amplitude of the point source, r_l ($l = 1, 2,\cdots, L$) denotes the different excitation point source positions, $\delta(r)$ denotes the Dirac function. $\eta\mu_{af}$ denotes the fluorescent yield to be reconstructed, where η denotes the quantum efficiency and μ_{af} denotes the absorption coefficient of the fluorescent probe.

To solve the coupled equations, the Robin-type boundary conditions (RBC) are implemented on the boundary $\partial\Omega$ of the domain Ω [17]:

$$2D_{x,m}(r)\partial\Phi_{x,m}(r)/\partial\vec{n}(r)+q\Phi_{x,m}(r)=0 \quad (r\in\partial\Omega) \tag{2}$$

where $\vec{n}$ denotes the outward normal vector to the surface $\partial\Omega$ and q is a constant depending on the optical reflective index mismatch at the boundary.

2.2 Finite element discretization

The finite element method is used to solve the DEs together with the boundary condition. The domain of the problem is discretized with tetrahedron elements and the base functions are treated as the test functions. Then the FMT problem can be linearized and the following matrix-form equations can be formed.

$$[K_x]\{\Phi_x\}=\{S_x\} \tag{3}$$

$$[K_m]\{\Phi_m\}=[F]\{X\} \tag{4}$$

with $F(i,j)=\int_\Omega\Phi_x(r)\psi_i(r)\psi_j(r)dr$.

$\Psi_i(r)$ and $\Psi_j(r)$ denote the base functions of the node i and node j, respectively; K_x and K_m denote the system matrix during excitation and emission, respectively. Φ_x and Φ_m denote the photon density on the finite element nodes during excitation and emission, respectively. S_x denotes the excitation light source distribution on the finite element nodes. Vector X, which is yet to be reconstructed, denotes the fluorescent yield on the finite element nodes.
Based on Eq. (4), the following linear relationship between the photon density Φ_m and the unknown fluorescent yield distribution can be established:

$$\{\Phi_m\} = [K_m^{-1}][F]\{X\} = [G]\{X\} \tag{5}$$

By removing the immeasurable entries in Φ_m as well as the corresponding rows in matrix G, the following equation is formed:

$$\{\Phi_m^{'}\} = [G^{'}]\{X\} \tag{6}$$

Then we assemble Eq. (6) for different excitation positions and the following linear relationship between the emitted fluorescence measurements Φ on the surface and the unknown fluorescent yield distribution X can be formed:

$$\{\Phi\} = [A]\{X\} \tag{7}$$

2.3 Reconstruction based on the spectral projected gradient pursuit method

To promote the sparsity of the solution, the l_1-norm regularization is incorporated into the FMT problem. Then, Eq. (7) can be transformed into the following form:

$$\underset{X}{\text{minimize}}\, f(x) = \|AX - \Phi\|_2 \ \text{ subject to } \ \|X\|_1 \le \tau \tag{8}$$

where τ denotes the regularization parameter. To solve the FMT problem, a method named spectral projected gradient pursuit (SPGP) was proposed to obtain a sparse solution to Eq. (8). It uses a projection operator defined as:

$$P_\tau(c) = \arg\min_x \|c - x\| \ \text{ subject to } \ \|x\|_1 \le \tau \tag{9}$$

This projection operator denotes the projection of a vector c onto the one-norm ball with radius τ. The proposed method was based on the directional pursuit framework. The new solution is estimated as $x_n = P_\tau(x_{n-1} - \alpha g_{n-1})$, where g_{n-1} denotes the gradient of the objective function and α denotes the step length. Thus the update direction of the proposed method is calculated to be $d_n = P_\tau(x_{n-1} - \alpha g_{n-1}) - x_{n-1}$. To evaluate whether the newly generated solution is appropriate for the problem, a nonmonotone line search strategy was introduced as follows:

$$\|r_n\|_2^2 \le \max_{0 \le j \le \min(n-1, L-1)} \|r_{n-1-j}\|_2^2 + \gamma (d_n)^T g_{n-1} \tag{10}$$

where r_n denotes the residual of the objective function and γ denotes the sufficient descent parameter. This strategy ensures that the objective function decreases sufficiently within L ($L \geqslant 2$) iterations. It is able to overcome some cases where the sequence of iterates follows the bottom of a curved narrow valley, which may occur in some specific optimization problems.

Then, in order to generate the new step length, the Barzilai-Borwein step length is introduced. It has the form as follows:

$$\alpha_{BB} = (\Delta x^T \Delta x) / (\Delta x^T \Delta g) \tag{11}$$

Where Δx denotes the increment of x_{n-1} between two consecutive iterations and Δg denotes the increment of the gradient g_{n-1} between two consecutive iterations. Then the new step length is calculated to be $\alpha_n = \min \{\alpha_{max}, \max [\alpha_{min}, \alpha_{BB}] \}$ in which α_{max} and α_{min} are two initial parameters. By using the Barzilai-Borwein step length, the convergence of this gradient method can be speeded up [18]. At last the halting conditions are used to determine whether to discontinue the proposed method or not. The main steps of the proposed method are summarized below:

Spectral Projected Gradient Pursuit Method

$x_0 = P_\tau[x]$, $r_0 = \Phi - Ax_0$, $g_0 = -A^T r_0$.
$n = 1$.
Outer Iteration:
(1) $\alpha = \alpha_{n-1}$

Internal Iteration :

(2) $x_n = P_\tau(x_{n-1} - \alpha g_{n-1})$

(3) $r_n = \Phi - A x_n$

(4) $d_n = x_n - x_{n-1}$

(5) **if** $\| r_n \|_2^2 \leqslant \max_{0 \leqslant j \leqslant \min(n-1, L-1)} \| r_{n-1-j} \|_2^2 + \gamma (d_n)^{\mathrm{T}} g_{n-1}$ **then**

(6) **Exit Internal Iteration**

else

(7) $\alpha = \alpha / 2$

end if

End Internal Iteration

(8) $g_n = -A^T r_{\mathrm{n}}$

(9) $\Delta x = x_n - x_{n-1}$; $\Delta g = g_n - g_{n-1}$

(10) $\alpha_{BB} = (\Delta x^T \Delta x)/(\Delta x^T \Delta g)$

(11) **if** $\Delta x^T \Delta g \leqslant 0$ **then**

(12) $\alpha_n = \alpha_{\max}$

else

(13) $\alpha_n = \min\{\alpha_{\min}, \max[\alpha_{\min}, \alpha_{BB}]\}$

end if

(14) $n = n+1$

(15) **if** halting condition true **then**

(16) **Exit Outer Iteration**

End if

End Outer Iteration

Output:

(17) $x = x_n$

3. EXPERIMENTS AND RESULTS

To evaluate the feasibility of the proposed method, numerical experiments were conducted in this section. The experiments were conducted based on a mouse-mimicking hetergeneous phantom, which was a cylinder and was 20 mm in diameter and 20 mm in height, as shown in Fig. 1. The phantom consisted of four kinds of materials representing bone (B), heart (H), lung (L) and muscle (M), as shown in Fig. 1(a). The optical parameters of the materials were listed in Table 1. To produce the fluorescence measurements, three fluorescent sources, which were spherical and were 2 mm in diameter, were centered in $z = 0$ plane and were placed in the left and right lungs, as shown in Fig. 1(b). The fluorescent yields of the sources were set to be 0.5. The black dots in Fig. 1(c) denote the excitation light sources, which were modeled as isotropic point sources located one mean free path of photon transport beneath the surface in $z = 0$ plane. For each excitation source, fluorescence measurements were obtained from the opposite cylindrical side with 160° field of view (FOV), as presented in Fig. 1(c). Fig. 1(d) demonstrated that the measured fluorescent data mapped onto the surface of the phantom. In order to reconstruct the fluorescent sources, the heterogeneous phantom was discretized into 3756 nodes and 21715 tetrahedron elements using the finite element method, as shown in Fig. 1(e). To better evaluate the feasibility of the proposed method, the conjugate gradient based method with l_2 norm (CG_L2) was used to reconstruct the same data sets [19]. All of the reconstructions were carried out on a personal computer with 2.39 GHz Intel Core 2 Duo CPU and 2 GB RAM.

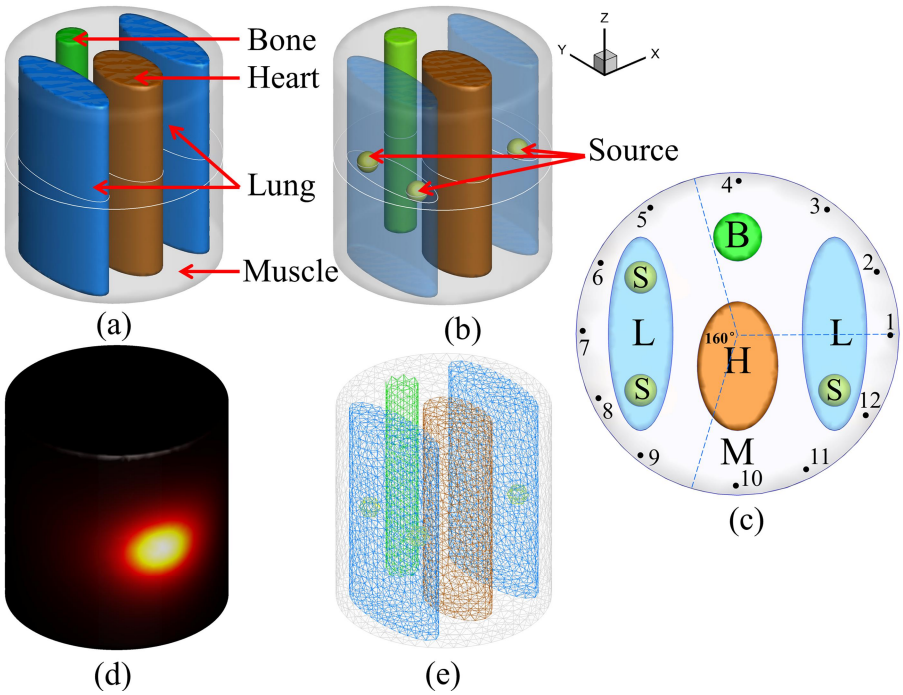

Fig. 1. The mouse-mimicking hetergeneous phantom for numerical experiments. (a) The 3D view of the mouse-mimicking hetergeneous phantom which consisted of four kinds of materials representing bone (B), heart (H), lung (L) and muscle (M). (b). The setup of the phantom for triple fluorescent sources. (c). The cross-section image of the phantom in the $z = 0$ plane. (d) The measured fluorescent data mapped onto the surface of the phantom. (e) The discretized heterogeneous phantom.

Table 1. The optical parameters of the mouse-mimicking hetergeneous phantom

Material	μ_{ax}(mm^{-1})	μ_{sx}(mm^{-1})	μ_{am}(mm^{-1})	μ_{sx}(mm^{-1})
Bone	0.0024	1.75	0.0035	1.61
Heart	0.0083	1.01	0.0104	0.99
Lung	0.0133	1.97	0.0203	1.95
Muscle	0.0052	1.08	0.0068	1.03

3.1 Evaluation of reconstruction accuracy

In the first experiment, fluorescence was excited by point sources from 12 different locations in sequence, as illustrated in Fig. 1. (b). Thus 12 measurement data sets were used to reconstruct the fluorescent sources. To simulate the real case, 5% Gaussian noise was added to these measurement data sets. CG_L2 method was used as the contrast method to verify the accuracy of the proposed method. Fig. 2 gives the reconstruction results of the CG_L2 method (a, b, c, d) and the proposed method (e, f, g, h). Fig. 1(a) and Fig. 1(e) demonstrate the 3D views of the reconstructed fluorescent sources in the phantoms. Fig. 1(b) and Fig. 1(f) give the 3D views of the reconstructed fluorescent sources assembled with the actual fluorescent sources. Fig. 1(c), Fig. 1(d), Fig. 1(g) and Fig. 1(h) demonstrate the corresponding slices images in the $z = 0$ plane. The green circles in the slice images denote the real locations of the fluorescent sources. The fluorescence intensity in Fig. 1(d) and Fig. 1(h) is normalized. From Fig. 2 we can clearly see that, the proposed method can recover the three fluorescent sources exactly. For each fluorescent source, the distance between the center of the actual fluorescent source and the center of the reconstructed fluorescent source is less than 1mm. However, the sources reconstructed by the CG_L2 method were over-smoothed due to the over-smoothing effect of the Tikhonov regularization and were not located in the right regions. Besides, the fluorescence reconstructed by the proposed method had a higher contrast to the background than the fluorescence reconstructed by the CG_L2 method, as shown in Fig. 1(d) and (e).

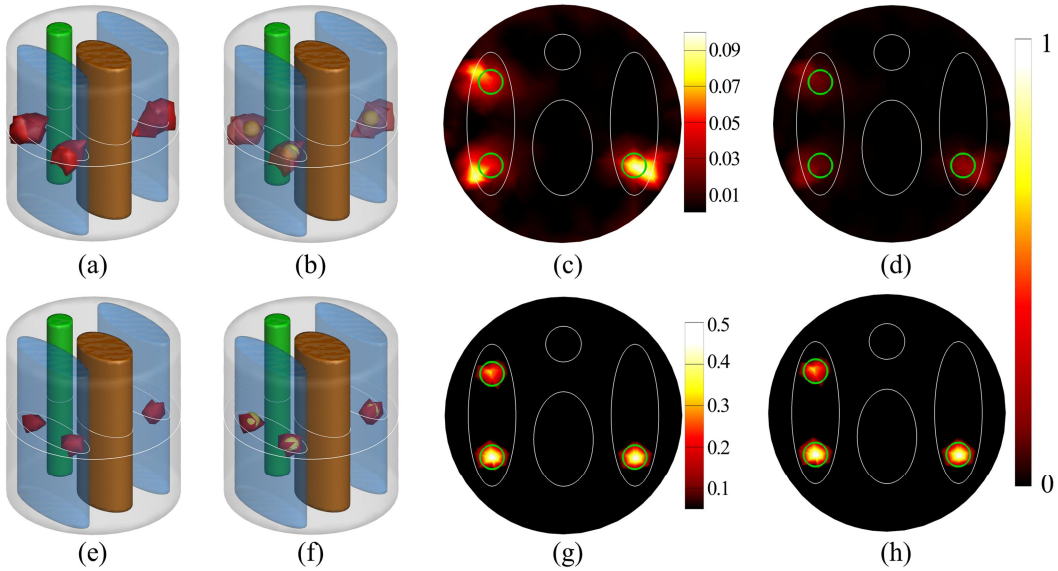

Fig. 2. The fluorescent yield reconstruction results by the CG_L2 method (a, b, c, d) and the proposed method (e, f, g, h). (a, e) The 3D views of the reconstructed fluorescent sources in the phantom. (b, f) The 3D views of the reconstructed fluorescent sources assembled with the actual fluorescent sources in the phantom. The actual fluorescent sources were indicated by the yellow spheres. (c, g). The corresponding slice images in the $z = 0$ plane. The green circles in the slice images denote the real locations of the fluorescent sources. (d, h). The slice images in the $z = 0$ plane. The fluorescence intensity in these images is normalized.

3.2 Evaluation of reconstruction efficiency

To examine the reconstruction efficiency of the proposed method, we compared the efficiency of proposed method with the CG_L2 method based on four different groups of data sets, which were presented on table 2. The sizes of the data sets were determined by the density of the discrete volumetric mesh. For the two reconstruction methods, the zero vector was used to initialize the unknowns. The results of the comparison are displayed in Table 2. It shows the time consumed by the proposed method as well as the contrast one for reconstructing the four groups of data sets. Each value of the reconstruction time was the average of ten independent runs.

From the results, we can clearly see that: 1. The proposed method worked more efficiently than the CG_L2 method when reconstructing the same data sets. 2. The proposed method became more computationally competitive as the size of the data set increases. 3. These data sets were discretized based on the mouse-mimicking hetergeneous phantom, which meant that our method was potential for practical applications.

Table 2. The efficiency comparison between the proposed method and the CG_L2 method. The size of the volumetric mesh equals the number of nodes multiplied by the number of tetrahedral elements.

No.	Volumetric mesh size	The proposed method (s)	CG_L2 method (s)
1	2970×16877	6.80	96.25
2	3756×21715	9.17	166.17
3	4650×26722	11.75	282.25
4	5255×30393	14.86	508.36

4. CONCLUSIONS

A new method based on spectral projected gradient pursuit was presented in this paper for FMT reconstruction. This method has introduced several strategies including the nonmonotone line search and the Barzilai-Borwein step length to guarantee the global convergence and simplify the computational complexity. To evaluate the proposed method, several heterogeneous simulation experiments were conducted. From the results, the conclusion could be drawn that the SPGP method was able to achieve satisfactory source localizations with a bias less than 1 mm; the computational efficiency of the method was one order of magnitude faster than the contrast method; and the fluorescence reconstructed by the proposed method had a higher contrast to the background than the contrast method. All the results demonstrated the potential for practical FMT applications with the proposed method.

5. ACKNOWLEDGEMENTS

This paper is supported by the National Basic Research Program of China (973 Program) under Grant No. 2011CB707700, the National Natural Science Foundation of China under Grant Nos. 81227901 and 61231004, the China Postdoctoral Science Foundation under Grant No. 2014M550881, the National Key Technology R&D Program of China under Grant No. 2012BAI23B01, and the Instrument Developing Project of the Chinese Academy of Sciences under Grant No. YZ201359.

REFERENCES

[1] C. Chi, J. Ye, H. Ding *et al.*, "Use of indocyanine green for detecting the sentinel lymph node in breast cancer patients: from preclinical evaluation to clinical validation," PloS one, 8(12), e83927 (2013).
[2] C. Chi, Y. Du, J. Ye *et al.*, "Intraoperative imaging-guided cancer surgery: From current fluorescence molecular imaging methods to future multi-modality imaging technology," Theranostics, 4(11), 1072 (2014).
[3] J. Ye, C. Chi, S. Zhang *et al.*, "A near-infrared fluorescence-based surgical navigation system imaging software for sentinel lymph node detection." 89351U-89351U-7.
[4] V. Ntziachristos, "Fluorescence molecular imaging," Annu. Rev. Biomed. Eng., 8, 1-33 (2006).
[5] V. Ntziachristos, C.-H. Tung, C. Bremer *et al.*, "Fluorescence molecular tomography resolves protease activity in vivo," Nature medicine, 8(7), 757-761 (2002).
[6] A. Ale, V. Ermolayev, E. Herzog *et al.*, "FMT-XCT: in vivo animal studies with hybrid fluorescence molecular tomography-X-ray computed tomography," Nature methods, 9(6), 615-620 (2012).
[7] J. Ye, C. Chi, Y. An *et al.*, "A fast and effective reconstruction method for fluorescence molecular tomography based on sparsity adaptive subspace pursuit," Proceedings of the SPIE, 8937, (2014).
[8] D. Wang, X. Song, and J. Bai, "Adaptive-mesh-based algorithm for fluorescence molecular tomography using an analytical solution," Optics express, 15(15), 9722-9730 (2007).
[9] W. Bangerth, and A. Joshi, "Adaptive finite element methods for the solution of inverse problems in optical tomography," Inverse Problems, 24(3), 034011 (2008).
[10] D. Han, J. Tian, K. Liu *et al.*, "Sparsity-promoting tomographic fluorescence imaging with simplified spherical harmonics approximation," Biomedical Engineering, IEEE Transactions on, 57(10), 2564-2567 (2010).
[11] D. Han, X. Yang, K. Liu *et al.*, "Efficient reconstruction method for L1 regularization in fluorescence molecular tomography," Applied optics, 49(36), 6930-6937 (2010).
[12] J. Shi, B. Zhang, F. Liu *et al.*, "Efficient L1 regularization-based reconstruction for fluorescent molecular tomography using restarted nonlinear conjugate gradient," Optics letters, 38(18), 3696-3699 (2013).
[13] J. Ye, C. Chi, Z. Xue *et al.*, "Fast and robust reconstruction for fluorescence molecular tomography via a sparsity adaptive subspace pursuit method," Biomedical optics express, 5(2), 387-406 (2014).
[14] D. Han, J. Tian, S. Zhu *et al.*, "A fast reconstruction algorithm for fluorescence molecular tomography with sparsity regularization," Optics express, 18(8), 8630-8646 (2010).
[15] N. Blow, "In vivo molecular imaging: the inside job," Nature Methods, 6(6), 465-469 (2009).
[16] A. Joshi, W. Bangerth, and E. Sevick-Muraca, "Adaptive finite element based tomography for fluorescence optical imaging in tissue," Optics Express, 12(22), 5402-5417 (2004).
[17] M. Schweiger, S. Arridge, M. Hiraoka *et al.*, "The finite element method for the propagation of light in scattering media: boundary and source conditions," Medical physics, 22(11), 1779-1792 (1995).
[18] M. Raydan, "The Barzilai and Borwein gradient method for the large scale unconstrained minimization problem," SIAM Journal on Optimization, 7(1), 26-33 (1997).
[19] J. Nocedal, and S. J. Wright, [Conjugate gradient methods] Springer, (2006).